Variations in cell plasticity and proliferation underlie distinct modes of regeneration along the antero-posterior axis in the annelid Platynereis

Loïc Bideau, Zoé Velasquillo-Ramirez, Loeiza Baduel, Marianne Basso, Pascale Gilardi-Hebenstreit, Vanessa Ribes, Michel Vervoort, Eve Gazave

Variations in cell plasticity and proliferation underlie distinct modes of regeneration along the antero-posterior axis in the annelid *Platynereis*

It takes guts to regenerate

Loïc Bideau[1], Zoé Velasquillo-Ramirez[1], Loeiza Baduel[1], Marianne Basso[1], Pascale Gilardi-Hebenstreit[1], Vanessa Ribes[1], Michel Vervoort[1†], Eve Gazave[1*]

[1] Université Paris Cité, CNRS, Institut Jacques Monod, F-75013 Paris, France

[†] Deceased

Correspondence to: Eve Gazave, eve.gazave@ijm.fr

Abstract:

The capacity to regenerate lost tissues varies significantly among animals. Some phyla, such as the annelids, display substantial regenerating abilities, though little is known about the cellular mechanisms underlying the process. To precisely determine the origin, plasticity and fate of the cells participating in blastema formation and posterior end regeneration following amputation in the annelid *Platynereis dumerilii*, we developed specific tools to track different cell populations. Using these tools, we find that regeneration is partly promoted by a population of proliferative gut cells whose regenerative potential varies as a function of their position along the worm's antero-posterior axis. Gut progenitors from anterior differentiated tissues are lineage-restricted, whereas gut progenitors from the less differentiated and more proliferative posterior tissues are much more plastic. However, they are unable to regenerate the stem cells responsible for the growth of the worms. Those stem cells are of local origin, deriving from the cells present in the segment abutting the amputation plane, as are most of the blastema cells. Our results favour a hybrid and flexible cellular model for posterior regeneration in *Platynereis* relying on different degrees of cell plasticity.

Key words:

gut progenitors, cell plasticity, metaplasia, blastema origin, regeneration, annelid, *Platynereis*

Introduction

Regeneration, the ability to reform a lost body part upon injury, is an essential process in animals. Its importance is illustrated by its wide deployment in metazoans, although the range of tissues that can be regenerated is highly variable from one species to another (Bely and Nyberg, 2010). While mammals can at best regenerate an organ, many other species can perform "extensive" regeneration such as the reformation of a limb (*e.g.* salamanders), a large amputated part of their body axis (*e.g.* annelids) or even their whole body from a small fragment of tissue (*e.g.* cnidarians, planarians) (Bideau et al., 2021). Despite this diversity, all regeneration processes go through three common steps: the formation of a wound epithelium enclosing the area of the injury, followed by the recruitment of progenitors at the wound site which often form a blastema (a mass of proliferative undifferentiated mesenchymal cells), and finally the growth of the blastema by cell proliferation and differentiation during a morphogenesis step (Galliot and Ghila, 2010; Tiozzo and Copley, 2015).

Uncovering the origin and fate of the cells contributing to blastema formation has been one of the greatest challenges in the field of regenerative biology for decades (Tanaka and Reddien, 2011). Studies of major regeneration models has established that the blastema can be formed by the progeny of activated progenitor or stem cells, as exemplified by the planarian *Schmidtea mediterranea,* whose regeneration is sustained by adult stem cells called neoblasts (Wenemoser and Reddien, 2010). As pluripotent cells (at least part of them), neoblasts participate in formation of all missing tissues (Wagner et al., 2011). Alternatively, the blastema can be formed by post-mitotic cells that dedifferentiate and re-enter cell cycle upon injury, as in the case in urodele limb regeneration (Stocum and Cameron, 2011). In this regenerative process, various local tissues close to the wound dedifferentiate into strictly lineage-restricted progenitors (Flowers et al., 2017; Kragl et al., 2009).

As such, two opposite models have been broadly defined: the first involves very highly plastic cells that migrate to the wound, the second involves local tissues that dedifferentiate to constitute a pool of diverse progenitors with low plasticity. However, the mechanisms of regeneration are often more

complex and in many species and contexts, both dedifferentiated cells as well as tissue-specific resident stem cells contribute to the blastema (*e.g.* axolotl limb regeneration, (Lin et al., 2021; Sandoval-Guzmán et al., 2014)).

Careful studies identifying the sources of blastema cells during regeneration are coming from few key regenerative model species but are lacking for the majority of regeneration-competent lineages. These models do not include representatives of the annelid phylum, which display substantial and diverse regenerative capacities. The majority of annelids can indeed regenerate their posterior and/or anterior parts upon amputation (Özpolat and Bely, 2016). Those regeneration processes have been studied for a long time and in various species (reviewed in (Bely, 2006)) but the precise cellular mechanisms involved in the formation of the blastema remain unclear.

The annelid *Platynereis dumerilii* is emerging as a useful and relevant model to address fundamental regeneration questions (Schenkelaars and Gazave, 2021; Özpolat et al., 2021). This marine worm has the ability, after embryonic development, to grow continuously by the addition of new segments in its posterior part, through a process of posterior elongation that relies on putative progenitor or stem cells localized in a subterminal growth zone (Gazave et al., 2013). Importantly, *Platynereis* has the astounding ability to regenerate its complex posterior end following amputation *via* the formation of a blastema and through stereotyped steps that we have previously defined (Planques et al., 2019). Upon amputation, the wound heals in 24 h (stage 1 at 1 day post amputation or 1dpa). One day later (stage 2, 2dpa), a small blastema has formed which rapidly grows. Between stages 2 and 3 (3 dpa), the blastema cells have started to differentiate into various tissues (*e.g.* muscles, nervous system…). At stage 3, the growth zone and the pygidium, which is the posterior-most part of the worm body, have begun to reform. At stage 5 (5 dpa), a new fully functional growth zone has been re-established and allows posterior elongation to resume (Planques et al., 2019).

The cellular and molecular mechanisms controlling this regeneration process are still largely unresolved. In our first study on this topic, we had shown, through S-phase cell labelling coupled with proliferation inhibition experiments, that cell proliferation is absolutely necessary from stage 2

onwards for regeneration to be properly achieved (Planques et al., 2019). Additionally, pulse-chase experiments suggested that most of the blastema cells have a local origin, from the segment abutting the amputation plane (Planques et al., 2019). The origin(s), plasticity and fate of the cells contributing to the regeneration blastema remains to be precisely determined.

In this study, we developed tools to track proliferative cells as well as gut epithelial cells. We determined that some gut cells from differentiated tissues constitute a population of progenitors uniquely contributing to the regeneration of gut epithelial cells. Strikingly, we also showed that upon posteriorization (*i.e.* by giving a posterior identity to previously anterior tissues), those lineage-restricted gut progenitors reveal a higher plasticity as they are also able to produce ecto/mesodermal derivatives through regeneration. However, they do not contribute to the regeneration of the growth zone stem cells, which are from local origin (*i.e.* from the segment abutting the amputation). These results argue for the existence of different degrees of plasticity, through regeneration, of intestinal progenitors along the antero-posterior axis of the animal.

Results

Cell proliferation patterns and cell cycle kinetics during continuous growth

Previous results have shown that cells proliferating in the context of normal continuous posterior growth may participate in the posterior regeneration in *Platynereis* (Planques et al., 2019). To further study the role of those cells during regeneration, we first examined the distribution of S-phase cells in non-amputated juvenile worms with EdU labelling. We exposed uninjured worms to EdU, either for 5 or 48h. An exposure of 5 h labels a pool of rapidly cycling cells (called hereafter “5h EdU+ cells”). In contrast, the 48h incubation labels a larger pool of cells including both rapidly and slowly cycling cells (called hereafter “48h EdU+ cells”). Such slowly-cycling cells have been shown to contribute to regeneration in several species including mammals (Karmakar et al., 2020; Koren et al., 2022) and

planarians (Molinaro et al., 2021). The distributions of EdU+ cells were examined immediately after EdU exposure both in whole samples (Fig. 1A-B') and in histological sections (Fig. 1C-D''). Three segments were examined, including the most posterior distinguishable segment (called Segment 1 or S1) (Fig. 1A', B', C'' and D'') as well as the sixth and seventh segments counted from the posterior region (called Segments 6 and 7 or S6 and S7, respectively) (Fig. 1A, B, C-D'). We observed many EdU+ cells in S1 regardless of the EdU incubation time (Fig. 1A', B'). S6 or S7 exhibit fewer labelled cells, especially the 5h EdU+ cells (Fig. 1A, B). We next looked more carefully at the localization of EdU+ cells within the tissues by performing semi-thin sections of S6 and/or S7 (transversal and longitudinal sections, Fig. 1C- D') and S1 (longitudinal sections, Fig. 1C'', D''). 5h EdU+ cells in S6/S7 mainly delineate the central and circular epithelium of what appears to be the gut (Fig. 1C, C') (Žídek et al., 2018; Dahlitz et al., 2023, Supp. Fig.1). However, in S1 the 5h EdU+ cells were located not only in the gut but also in ectoderm and mesoderm (Fig. 1C''). In contrast, 48h EdU+ cells were found in all trunk tissue subtypes in S1, S6 and S7 (Fig. 1D to D").

To better assess those different populations of proliferating cells, we performed cell cycle kinetics analyses. To determine if the proliferative cells behave differently as a function of their location along the antero-posterior axis of the animal or depending on their specific tissue, we implemented a cumulative EdU labelling assay (Nowakowski et al., 1989). This method relies on the sequential administration of a thymidine analog, here the EdU, until all proliferative cells are labelled, allowing one to determine the total cell cycle length (Tc), S-phase length (Ts) and growth fraction (GF or proportion of cycling cells). We applied it to calculate such cell cycle parameters in different segments (S1, S6 and S7) and in different tissues (gut *versus* the other trunk tissues) (Fig. 1E, F and G; Supp. Table 1 and 2). We found, regardless of the tissue examined, many more cells are cycling in S1, compared to S6 and S7. Regarding the gut, the GF of 38 % in S1 decreases to 29% and 28% in S6 and S7 respectively. For the rest of the trunk tissues, 63 % of cells are cycling in S1, while this rate drops to 18% and 15% in S6 and S7 respectively (Fig. 1G; Supp. Table 1 and 2). We also determined that the gut cells, whatever their locations, are cycling more quickly than the other trunk tissue cells. Indeed, the cell cycle length

(Tc) for the S1 gut cells is of 27 h while the other cells have a Tc of 54 h. Similarly, in S6 and S7, the gut cells Tc is 50 h and 49 h *versus* 62 h and 66 h for the other cells in the trunk (Fig. 1G; Supp. Table 1 and 2). In addition, the S-phase length (Ts) is broadly similar between the gut cells and other cell types at positions S6 and S7 (15 h *versus* 14 h and 16 h *versus* 19 h). In contrast, for the S1, the Ts is drastically shortened for the gut cells (3 h *versus* 20 h) (Fig. 1G; Supp. Table 1 and 2).

In summary, the proportion of cycling cells (or GF) varies along the antero-posterior (AP) body axis of the uninjured worms, with more proliferative cells in posterior segment that in anterior ones (Fig. 1A, A', B, B' and G). In addition, the proportion of cycling cells varies according to the tissue type, with the anterior gut cells remaining highly proliferative with a faster cell cycle, compared to the other tissues.

Posterior regeneration is fuelled by cells proliferating before amputation

Next, we aimed to determine the respective contribution of these populations of cycling cells to posterior regeneration. We incubated worms with EdU for 5h or 48h, as previously, and amputated them at two different positions (Fig. 2A), called amputation "0" (if the cut was made just behind S1, removing only the pygidium, the growth zone) or amputation "-5" (if the cut was made just behind S6, removing five recognizable segments in addition to the terminal part. After 5 days of regeneration, the patterns of EdU+ cells in the regenerating parts were determined (Fig. 2B-E'). After a 5h-long EdU pulse followed by an amputation "-5", only 9 % of the blastema cells were EdU+ (Fig. 2F; Supp. Table 1) and these appeared to be located mostly within the regenerating gut (Fig. 2B, B'). After a 5h-long EdU pulse followed by an amputation "0", 19% of the blastema cells were EdU+ (Fig. 2F; Supp. Table 1) and they were located not only in the gut but also in mesodermal and ectodermal tissues (Fig. 2D, D'). In contrast, after a 48h-long EdU pulse, more than 70% of the blastema cells were EdU+, regardless where the amputation was performed (amputation "-5" or "0") (Fig. 2F; Supp. Table 1) and located in all tissue types (Fig. 2C, C' and E, E'). These results indicate the cells contributing to regeneration, whether from the anterior or posterior parts of the worms, are predominantly those that had been cycling prior to amputation.

Interestingly, almost all the blastema cells originate from 48h EdU+ cells in both anterior (S6/S7) and posterior (S1) segments. 5h EdU+ cells also contribute to a far lesser extent. In the posterior-most segment (S1), 5h EdU+ cells produce derivatives in all cell compartments while in anterior segments (S6/S7), they contribute mostly to the regeneration of gut cells. Those differences in patterns of EdU+ cells within the blastema reflect the initial patterns of cycling progenitors labelled with a short pulse of EdU in the segments abutting the amputation plane (Fig. 1A, A', C-C''), *i.e.* distributed in all cell compartments in the posterior-most segment and mostly localized within the gut in anterior segments. We aimed to better understanding the particular contribution of these 5h EdU+ cells in anterior segments, to regeneration. First, to confirm their gut identity we coupled EdU labelling (*i.e.* after a 5h-long EdU pulse followed by an amputation "-5") with *in situ* hybridizations for the gut specification factor *foxA* (Fig. 2G) and the smooth muscle marker *calponin* (Fig. 2H), (Brunet et al., 2016). The majority of the EdU+ cells (60 %) colocalizes with *foxA* inside the regenerating gut (Fig. 2G, G', Supp. Table 1) while only very few EdU+ cells colocalize with *calponin*, most of which were inside the gut embedded in smooth muscles (Fig. 2H, H'), thus confirming their gut identity. To go further into the characterization of these potential gut progenitors, we performed *in situ* hybridizations on sections (at the anterior position S6) for several markers of the germline multipotency program (or the GMP signature), a set of genes expressed in adult multi/pluripotent stem cells and progenitors, in many metazoan species (Juliano et al., 2010). We observed the expression of GMP genes *Myc, PiwiB* and *Vasa* in a large subset of gut cells (Supp. Figure 1C to E), some of them being proliferative 5h EdU+ cells (Supp. Figure 1F).

In summary, this study identify an important pool of cycling gut progenitors cells in anterior segments, present before amputation, that express a pool of markers found in stem/progenitor cells, and that contribute to posterior regeneration and give rise to functional differentiated gut cells.

Tracing anterior gut cells with fluorescent beads demonstrates their lineage restriction during regeneration

To further explore the contribution of anterior gut progenitors to regeneration, we developed a means to specifically label gut epithelial cells. Worms incubated with 1µm-diameter fluorescent beads would ingest them and they would specifically incorporate within nearly all the gut epithelial cells (Fig. 2I-I'') excepting the last few posterior segments (Fig. 2I). With this technique, we could then precisely determine the contribution of gut epithelial cells over the course of regeneration (5 stages) following anterior amputation (Fig. 2J1-J5'). At stage 1, when the wound epithelium has formed, beads-labelled cells could be found within the segment abutting the amputation where the gut has retracted (Fig. 2J1, J1'). As soon as the blastema has formed at stage 2 (Fig. 2J2, J2'), the fluorescent beads were found inside the regenerating gut consistent with anus reformation. During the later growth and differentiation phases (stages 3 to 5) the fluorescent bead signal remained restricted to the gut epithelium (Fig. 2J3-J5, 2J3'-J5'). At stage 5, combining the previous EdU labelling experiment (EdU+ cells in the regenerative part coming from the cycling gut progenitors, cf. Fig. 2B), with the fluorescent beads (Fig. 2K, K'), we found overall colocalization of the two labels confirming the congruence of the two methods for labelling the gut cells as well as confirming their particular contribution to blastema gut cells.

We conclude that gut progenitors in anterior segments of unamputated worms contribute exclusively to posterior regeneration of the gut epithelium, and are thus lineage-restricted.

Posterior gut cells are plastic and give rise to several cell lineages during regeneration

To assay the lineage-restriction, if any, of the gut from the posterior-most segment, we first had to find a way to label them, since the posterior-most gut epithelial cells are unable to incorporate fluorescent beads (Fig. 2I) and since a 5h-long EdU pulse labels many progenitors outside the gut in posterior segments (Fig. 1A', C''). We overcame this problem by performing two sequential rounds of amputation on worms whose anterior gut progenitors are labelled with a 5h-long EdU pulse or with fluorescent beads. After the first round, the regenerated gut of the posterior segments had

incorporated descendants of the bead/EdU-labelled cells from the anterior gut. These worms could then be subjected to a second amputation (see Fig 3A ; details in the Methods).

Using this procedure, we observed differences in the distribution of beads-labelled (Fig. 3B) or EdU+ cells (Fig. 3C) along the antero-posterior axis of the "blastema-like" structure (*i.e.* a structure composed of a mix of a 10 dpa (anteriorly) and a 5 dpa (posteriorly) regenerated structure). In the anterior part, which corresponds to the remaining tissues of the 1st regeneration, the fluorescent beads and the EdU+ cells were still specifically or mainly restricted to the gut, respectively (Fig. 3B', C'). Strikingly, however, in the posterior part of the blastema-like structure, which corresponds specifically to the 2nd regeneration event, fluorescent beads and EdU+ cells were detected both inside and outside the gut, mainly in the dorsal side of the regenerating part (Fig. 3B'', C'', white arrows). Moreover, there were significantly more EdU+ cells in the posterior part (23.8%, Fig.3D, Supp. Table 1) than in the anterior part (17.4%, Fig. 3D, Supp. Table 1). Similarly, the number of BrdU+ and EdU+/BrdU+ cells were higher in the posterior part of the structure than in the anterior part (Fig. 3D, Supp. Table 1). This means that the gut progenitors, previously labelled with EdU, are actively mobilized during the 2nd regeneration and seem to contribute to the formation of tissues other than the gut, and more than a third of them are still proliferative. In addition, highly proliferative cells participating in the 1st regeneration labelled with BrdU, contribute massively to this 2nd event of regeneration as well (Fig. 3C to C'', D, Supp. Table 1)

We then determined the molecular identity of the cells originating from the gut progenitors that we observed outside the gut after the 2nd regeneration (Fig. 3B'', C'') by coupling EdU labelling and *in situ* hybridizations for tissue-specific genes (Fig. 3E-I'''), including: the gut specification factor *foxA* (Fig. 3E to E"), the smooth muscle marker *calponin* (Fig. 3F to F"), the pygidial marker *caudal* (Fig. 3G to G"), the neural progenitor factor *neurogenin* (Fig. 3H to H") and the ectodermal growth zone stem cell marker *hox3* (Fig. 3I to I"'). In the anterior part of the "blastema-like" structure, EdU+ cells mostly colocalize with *foxA* endodermal expression and are encompassed by the mesodermal expression domain of *calponin*, similar to the patterns obtained earlier for the 1st regeneration (Fig. 3E', F'; Cf. Fig.

2G-H'). In contrast, in the posterior part of the "blastema-like" structure, many EdU+ cells did not colocalize with *foxA* but did with *calponin* (Fig. 3E'', F'', white arrows). Some of the EdU+ cells also expressed *caudal* within the mesoderm and the ectoderm of the regenerating pygidium (Fig. 3G'', white arrow). In contrast, we never observed any colocalization with the *neurogenin* expression domain (Fig. 3H'') in the ventral neurectoderm. Similarly, the EdU+ cells did not colocalize with the ventral part of *hox3* expression domain in the ectodermal growth zone (Fig. 3I, I'''). In the dorsal part of *hox3* expression domain, the presence of a very few EdU+ cells cannot be ruled out (Fig. 3I'').

Taken together, these results argue that the gut cells have acquired plasticity upon posteriorization. These results support the idea that the gut progenitors within the posterior-most segments may display such plasticity compared to their anterior lineage-restricted counter parts. It suggests the presence along the AP axis of different degrees of cellular plasticity positively associated with the amount of proliferation of the tissues we documented above.

Cell migration and proliferation as well as tissue maturity regulate gut cell plasticity

This intriguing plasticity harboured by posterior gut progenitors is *de facto* spatially limited. Indeed, we showed that anteriorly-located gut progenitors are lineage-restricted. Their plasticity is thus apparently lost upon growth and differentiation of the tissues. We aimed here at describing the cellular mechanisms underlying this plasticity; and also, at determining at which point the posteriorized gut progenitors would lose it. As cell proliferation and migration are often required in similar processes (Friedl and Gilmour, 2009), we hypothesized it would be the case here as well. To this end, we performed the same reamputation procedure, but experimentally inhibiting cell proliferation with Hydroxy-Urea (HU) or cell migration with the actin inhibitor LatrunculinB (LatB, (Spector et al., 1983), used for instance to inhibit leukocyte migration (Lerchenberger et al., 2013; Yan et al., 2019)) during the second phase of regeneration (Fig. 4A). Previous results have shown that the inhibition of cell proliferation with HU does not prevent the formation of the blastema but hinders its growth and differentiation (Planques et al., 2019). The inhibition of cell migration (and modifications of cell shape)

with LatB slows down regeneration and causes mild morphological defects (thicker anal cirri, Supp. Fig. 2A, B). In contrast to the controls in which EdU+ cells are found, as expected, outside the gut in the posterior region of the blastema-like structure (Fig. 4B-B", white arrow), when inhibiting cell migration with LatB, most EdU+ cells stayed mostly restricted inside the gut in both anterior and posterior parts of the "blastema-like" structure (Fig. 4C to C''). To ensure that the regeneration slowdown observed following treatment with LatB was not due to an indirect alteration of cell proliferation (Supp. Fig. 2B, C), we made a short EdU pulse in LatB-treated and DMSO-control samples at 5dpa and found a similar percentage of EdU+ cells in both conditions (Supp. Fig. 2B). A pulse of EdU at 2dpa, followed by a chase until 5dpa, demonstrated that cells do divide in both conditions (Supp. Fig. 2C). We concluded that LatB does not affect cell proliferation, as cells are neither blocked in S-phase nor in M-phase, and that the restriction of EdU+ cells to the gut is due to cell migration defects. Similarly, most EdU+ cells are restricted inside the gut in the "blastema-like" structure when inhibiting cell proliferation with HU (Fig. 4D-D'').

To determine at which point the posteriorized gut progenitors lose their enhanced plasticity, we performed the reamputation procedure, but at later stages of initial regeneration (*i.e.* at 9dpa or 12dpa, instead of 5dpa) when newly produced tissues are differentiating (Fig. 4A). We observed that, as expected, the distribution of EdU+ cells is mostly restricted inside the gut in the anterior part of the regenerating structure (1st regeneration, Fig. 4 E, E', F, F') but also in its posterior part (2nd regeneration, Fig. 4E, E'', F, F''), showing that posteriorized gut progenitors have lost plasticity at those stages.

We conclude that cell proliferation and the cellular functions dependent on actin are crucial for the posteriorized gut progenitors to acquire their plasticity, and that this plasticity is lost very quickly upon maturation of the tissues.

Most of the blastema cells are of local origin, including the regenerated posterior stem cells

The above experiments showed that, whatever their position along the antero-posterior (AP) axis of the worms, the gut progenitors only comprise part of the blastema, even the plastic posteriorized gut

progenitors. The anterior gut progenitors provide only blastema gut cells, and the posterior ones, while producing several derivatives, probably do not regenerate neural tissues (Fig. 3H) and can only at best regenerate few stem cells of the growth zone (Fig. 3I). This raises questions about the origin of the cells that will give rise to the rest of the tissues, and, in particular, the stem cells of the regenerated growth zone. Additionally, as the position of the gut progenitors along the AP axis impacts their fate, could this be the case as well for the other cells participating in the blastema formation? Our previous work showed that most of the blastema cells are of local origin, from the segment abutting the amputation plane, in a context of an anterior amputation (*i.e.* amputation "-5", (Planques et al., 2019)). We thus sought to determine whether the source of the regenerative cells would remain local along the AP axis and also whether the stem cells of the growth zone would be of local origin as well. To distinguish local *versus* more distant tissues contributions to the regeneration along the body axis, we used an experimental set-up consisting in two serial amputations performed either in anterior ("-5") or posterior ("0") locations (Fig. 5 and Supp. Fig. 4; and Supp. Fig. 3, respectively) (see Planques et al., 2019). First, to have a proxy for the cells activated by anterior or posterior amputation, we performed a 5h-long EdU pulse at stage 1 when regeneration has been initiated and the wound epithelium formed (Fig. 5A), chased the EdU for two days (*i.e.* until 3 dpa) and performed a 1h-long BrdU pulse before collecting the samples. We determined that 53% of the blastema cells (at 3dpa for an anterior amputation) arose from those EdU+ cells proliferating after amputation (Fig. 5B). Moreover, they contribute massively to the pool of highly proliferative cells at 3dpa (among the 32 % of BrdU+ cells, 80% of them are also EdU+), which means that those EdU+ cells participate not only in the formation of the blastema but also in the subsequent phases of regeneration. Thus, they harbour a high regenerative potential. We wished to quantifying the precise difference of regenerative potential of the EdU+ cells in the segment abutting the amputation plane with those in the segment directly anterior to it, for the two positions of amputations (anterior *versus* posterior). We amputated worms anteriorly (see Fig. 5) or posteriorly (see Supp. Fig. 3) and let them regenerate for 24h, performed a 5h-long EdU pulse to label the cells activated by the amputation and let the worms regenerate two

more days when the blastema has formed. Then, we either amputated the blastema and the first abutting segment (Amputation A) or only the blastema (Amputation B). Following this second amputation, we let the worms regenerate three more days until another blastema had formed, and performed a 1h-long BrdU pulse before collecting the samples to quantify how many EdU+ are still proliferative after both amputations (Fig. 5A).

We found that the number and localization of BrdU+ cells are similar between condition A (Fig. 5C, Supp. Fig 3A) and B (Fig. 5D, Supp. Fig 3B; roughly 33 %, see individual values in Fig. 5G and supp. Fig 3C), whatever the position of the amputation (anterior *versus* posterior). In contrast, we obtained very different EdU+ cell patterns in the blastema depending on the second amputation condition (A *versus* B). For an anterior amputation, in condition A, only around 7% of internal cells are EdU+ (Fig. 5C, C', G; Supp. Table 1) whereas in condition B, around 69 % of the blastema cells are EdU+, in both superficial and internal tissues (Fig. 5D, D', G; Supp. Table 1). The situation is similar for a posterior amputation: while in condition A, around 27 % are EdU+ (Supp. Fig. 3A, A', E), around 75 % of the blastema cells are EdU+ in condition B (Supp. Fig. 3B, B', E). Interestingly, roughly 40% of the EdU+ cells are BrdU+ at 3 days post-2nd amputation in all conditions (Fig. 5C, D, G; Supp. Fig. 3A, B, E; Supp. Table 1).

Given that the only difference between conditions A and B is the absence or the presence of the segment abutting the first amputation plane, we conclude from these experiments that the cells activated by the amputation and located close to the wound have a higher plasticity than the ones located more anteriorly. They thus contribute to most of the blastema cells, regardless the site of the initial amputation (anterior *versus* posterior).

We next sought to determine the origin of the stem cells of the regenerated growth zone, and more precisely whether they would be of local origin as well, all along the AP axis. To track the regenerated stem cells, we relied on the fact that they constitute a population of Label Retaining Cells (LRC, (de Rosa et al., 2005)). As putative stem cells, their proliferation rate is rather low and consequently after an EdU incorporation the signal should be retained longer than in other cell types. We used the same experimental set-up as described above, but instead of collecting the samples after the 1h-long BrdU

pulse, we chased both the EdU and BrdU by letting the worms regenerate for four more days, until the very end of the regeneration process (Fig. 5A). For an anterior amputation, as expected, the pattern of BrdU+ cells is similar between conditions A and B (Fig. 5E, E', F, F' and G; Supp. Table 1). In contrast, the patterns of EdU+ cells are very distinct between both conditions. In condition A, there are still very few EdU+ cells (6%, Fig. 5G; Supp. Table 1) scattered in internal tissues (Fig. 5E, E'). As for condition B, there is a dramatic 4-fold reduction of the proportion of EdU+ cells in the samples (from around 69 % to 17 %, Fig. 5F, G; Supp. Table 1). This reflects the fact that most of the blastema cells underwent enough cell divisions to dilute the EdU signal. The remaining 17 % of EdU+ cells appear localized primarily at the interface between the pygidium (the terminal part of the worm body) and the new growing segments which presumably corresponds to the regenerated growth zone stem cells (Fig. 5F, F'). This EdU pattern is what could be expected for an LRC. A similar experimental approach has been followed after an initial posterior amputation (Fig. 5A). In this case, there are higher proportions of EdU+ cells in both conditions (17.9% for condition A and 36.2% for condition B, Supp. Fig. 3C, D, E) but similarly EdU+ cells do not appear to be located in the growth zone in condition A whereas they are in condition B (Supp. Fig. 3C-D'). The higher proportions of EdU+ cells for both conditions (A and B) for an amputation "0", compared to an amputation "-5" may reflect more proliferation in the tissues abutting a first initial posterior amputation than in more anterior tissues.

To confirm the localization and identity of those LRCs, we coupled EdU labelling with whole-mount *in situ* hybridizations for markers of different cell populations of the growth zone (Gazave et al., 2013). We selected the genes *hox3* and *evx* – expressed in the ectodermal cells of the growth zone, as well as *piwiB*, expressed in both the ectodermal and mesodermal cells of the growth zone (Fig. 5 and Supp. Fig. 4). After an initial anterior amputation, in condition A, the few remaining internal EdU+ cells do not colocalize with *hox3* signal (Fig. 5H, H') whereas they do colocalize in condition B (Fig. 5I, I', white arrow). Similar results were obtained for *evx* (Supp. Fig. 4A- B') and *piwi* (Supp. Fig. 4C-D').

These results demonstrate that the stem cells of the regenerated growth zone originate from local cells (*i.e.* from the segment abutting the amputation plane) activated by the amputation, whether this

amputation has been performed anteriorly or posteriorly along the animal body axis. In addition, those cells have a higher plasticity compared to those located more distantly to the amputation plane (*i.e* one segment upstream).

Discussion

Homeostatic progenitors with accelerated cell cycle are a cellular source for regeneration

Our proliferation labelling experiments revealed the contribution of both gut and non-gut progenitors from non-amputated tissues in *Platynereis* posterior regeneration. Importantly, the progenitors from the non-gut anterior trunk tissues, which are cycling more slowly than the gut progenitors, give rise to the great majority of the blastema cells. Slowly-cycling stem/progenitor cells are the main source of regenerative cells in other contexts of regeneration in many species. In mammalian skin (Koren et al., 2022) and gut (Karmakar et al., 2020) regeneration, they are critical for wound repair. Similarly, they are involved in whole-body regeneration in planarians (Molinaro et al., 2021) or in the ctenophore *Mnemiopsis leidyi* (Ramon-Mateu et al., 2019), as well as in head regeneration in the cnidarian *Hydra* (Govindasamy et al., 2014). Usually the cell cycle of those slowly-cycling progenitors has to accelerate to produce the cells required for regeneration. This can be achieved through either the acceleration of their S phase (as in *Drosophila* imaginal disc regeneration, (Crucianelli et al., 2022)) or the shortening of their G1 phase (as in *Drosophila* gut regeneration, (Cohen et al., 2021)).

In *Platynereis*, the cell cycle length in progenitors from the anterior non-gut tissues does not correlate with the timing of tissue reformation during posterior regeneration. In fact, it requires 62 h for the non-gut progenitors to cycle, during which time, a large highly proliferative blastema has already formed (Planques et al., 2019). Thus, only a cell-cycle acceleration can explain their massive contribution to the blastema. While we now have data about cell cycle kinetics in non-amputated tissues, precise measurement of the cell cycle parameters during regeneration in *Platynereis* remains

to be performed. Nonetheless, the identification of these two types of progenitors was decisive for a better understanding of the cellular sources of posterior regeneration in *Platynereis*.

A cellular model for posterior regeneration in *Platynereis*

In this study, we aimed to establish a model of regeneration for the annelid *Platynereis* at the cellular level. We first obtained new insights on the fate of the cells participating in the regeneration. We highlighted different degrees of plasticity of gut progenitors during regeneration by showing that, in contrast to their lineage-restricted anterior counterparts, posterior gut progenitors can widen their range of cell fate during regeneration and produce ecto/mesodermal derivatives. These different degrees of plasticity were shown to be positively associated with the levels of proliferation of the tissues, with the most proliferative tissues being localized posteriorly. As those posterior-most tissues close to the growth zone are also the most -recently formed, we can presume that anterior tissues are generally more differentiated than posterior ones. This intuitive assumption for a continuously growing animal has some experimental support. For instance, posterior-most segments never possess chaetae (extracellular structures produced by mature parapodia) nor do they express the chaetae-associated gene marker (*Chitin Synthase*) (Gazave et al., 2017). Similarly, they do not contribute to gas exchanges, as they never express globin markers (Song et al., 2020), nor to efficient digestion, as revealed by their inability to incorporate beads (Fig. 2I). Thus, the different levels of plasticity and proliferation our study uncovered may be negatively associated with the degree of tissue differentiation.

It was shown previously in *Platynereis* that most of the blastema cells arise locally, from the segment directly abutting the amputation plane (Planques et al., 2019). We confirmed and extended this finding by determining that most blastema cells, including the stem cells of the regenerated growth zone, are of local origin whatever the level of differentiation of the segment abutting the amputation plane (*i.e.* anterior or posterior tissues).

Two broad strategies have been proposed for tissue regeneration in various contexts (Bideau et al., 2021). In one, there are pre-existing resident pluripotent stem cells that can migrate to the wound site and initiate formation of the missing tissue as in the planarian *Schmidtea mediterrannea* or the cnidarian *Hydractinia symbiolongicarpus* (Wagner et al., 2011; Varley et al., 2023). The existence of adult stem cells (pluripotent or with less potency) in regeneration has been proposed (with little evidence) in many annelids, including earthworms (*Lumbriculus* sp. and *Enchytraeus japonensis* (Randolph, 1892; Myohara et al., 1999; Sugio et al., 2012), or *Capitella teleta,* (de Jong and Seaver, 2017). In addition, a recent single cell atlas for another species, *Pristina leidyi* suggests the existence of such stem cells with a pluripotency signature, but their role during regeneration remains to be established (Álvarez-Campos et al., 2023). While we cannot definitely rule out this possibility, our data does not support the idea that adult multi/pluripotent stem cells are involved during posterior regeneration in *Platynereis*.

In the other strategy, differentiated cells close to the wound undergo a partial dedifferentiation, forming lineage-restricted cells that can repair the injury , *e.g.* in the salamander limb regeneration (Kragl et al., 2009). Dedifferentiation was also proposed for a couple of annelid species (*i.e. Syllis malaquini* (Ribeiro et al., 2021) or *Alitta virens* (Shalaeva and Kozin, 2023)) during posterior regeneration. So far, the cellular trajectories supporting this idea remain unclear but such data already highlight the likely diversity of cellular mechanisms of regeneration within annelids (Bely, 2014).

Our data led us to define a hybrid cellular model (Fig. 6) for *Platynereis* posterior regeneration*:* most of its regenerative cells have a local origin, but the massive contribution of slowly-cycling progenitors rules out the possibility of a “complete” dedifferentiation process in which post-mitotic cells re-enter cell cycle. Rather, our results support the idea of pools of specialized progenitors with different replication rates, maintained throughout juvenile stage, that are mobilized upon an amputation trigger. Among them, posterior gut progenitors can become plastic during regeneration.

Plasticity of gut progenitors in *Platynereis* as an example of metaplasia during regeneration

Seminal studies of embryonic development led to the formalization of a broad model in which cell differentiation is an irreversible process, and development as a whole constitutes a gradual loss of potency from the totipotent zygote to fully differentiated adult cells (Caplan and Ordahl, 1978; Merrell and Stanger, 2016). This inflexibility of cell identity is currently being reconsidered in the light of recent genetic lineage tracing experiments, which have uncovered various developmental processes showing metaplasia*,* the acquisition of cell identities that are unusual for a given tissue (Virchow, 1886; Mills et al., 2019). Metaplasia was often observed during various regeneration contexts in which progenitor/stem cells can acquire a higher plasticity compared to tissue homeostasis, even though it is always limited in terms of potency and temporality. For instance, in the zebrafish fin, specific subpopulations of fibroblasts can restore more types of fibroblasts during regeneration than they do during homeostasis, but they can only produce fibroblasts (Tornini et al., 2017). Likewise, in mammals, a skin injury can transiently widen the progeny of specific skin stem cells which can then produce all the diversity of skin cells but not cells outside the skin (Blanpain and Fuchs, 2014).

In this study, we uncovered the intriguing ability for posterior less differentiated gut progenitors to produce other types of derivatives (*e.g.* epidermis or muscle) during regeneration, which can be considered as an example of metaplasia as well. Interestingly, the metaplasia of the gut in *Platynereis* is also limited in different ways. It is rather transitory; metaplasia probably stops as soon as the gut starts to differentiate. Related to this, it is also limited spatially in the body of the animal: only newly-produced (and therefore posterior) gut progenitors can switch lineage during regeneration. Moreover, this metaplasia is only partial, as posterior gut progenitors likely do not produce nervous system or putative posterior stem cells.

Why are posterior gut progenitors with enhanced plasticity unable to produce nervous system derivatives upon amputation? In many annelids, the ventral nerve chord (VNC) from non-amputated tissues plays a major role in the formation of the nervous system in the regenerated structure (Sinigaglia and Averof, 2019). In *Platynereis*, nerves from the VNC will rapidly innervate the blastema (Planques et al., 2019) and may serve as both direct and indirect source of signals (Boilly et al., 2017).

Perhaps such posterior gut progenitors cannot replace this important signal as well as the physical support provided by the VNC, in contrast to muscle cells which appear *de novo* in the blastema and do not seem to rely on the muscle system in non-amputated tissues for their initial differentiation (Planques et al., 2019).

Upon amputation, posterior gut progenitors also never produce the putative posterior stem cells responsible for the constant growth of the worms (Gazave et al., 2013). We can imagine that "enhanced" posterior gut progenitors are unable to produce stem cells as the latter may possess a too high potency, unreachable through their metaplasia. However, our results indicate that other cells (whose identity remains to be determined) located in the segment abutting the amputation plane can reach such potency to produce posterior stem cells. As such, the gut is not the only tissue capable of metaplasia following the amputation signal. It would be interesting to determine whether this metaplasia is specific to given types of tissue or if it depends solely on the degree of differentiation of any tissue.

Posterior regeneration in *Platynereis* is a plastic process at the cellular level but is morphologically robust

This phenomenon of metaplasia of posterior gut cells highlights an important point regarding the cellular processes involved during regeneration. Indeed, different sources of cells along the antero-posterior axis of the animal contribute to the blastema and eventually to a morphologically identical structure. This notion of different cellular "paths" for a same regeneration process is intriguing and rather uncommon. One key akin example is the retinal regeneration of *Xenopus* in which the involvement of three different cellular sources has been reported, depending on the extent of the injury (Parain et al., 2023). So far, we have no idea about the molecular mechanisms underlying such diversity of cellular mechanisms for regeneration.

In addition, those results led us to consider the robustness of the posterior regeneration in *Platynereis*. In a previous study, we reported that serial amputations (up to 10) do not impair regeneration

efficiency, at least at the morphological level (Planques et al., 2019). Similar robust regeneration events after successive injuries exist in some species, such as the zebrafish fin (Azevedo et al., 2011) and the newt's lens that can properly regenerate even after 18 repeated lens removal spanning over 30 years (Eguchi et al., 2011), without any modification of the associated transcriptional program (Sousounis et al., 2015). In contrast, in other species, the succession of injuries does reduce regeneration effectiveness (Eming et al., 2014) by either exhausting the tissue-specific stem cell pool (*e.g.* in the mouse lung epithelium (Ghosh et al., 2021) or the *Drosophila* gut epithelium (Haller et al., 2017)), or through the misexpression of regeneration initiation genes (*e.g*. in the axolotl limb, (Bryant et al., 2017)). We can hypothesize that the different cellular paths for regeneration depending on the localization, proliferation and differentiation levels of the tissues are important for the morphological robustness of the process.

Material and methods

Platynereis dumerilli breeding culture, amputation procedure and biological material fixation (whole mount)

P. dumerilii juvenile worms were obtained from a husbandry established in the Institut Jacques Monod (for breeding conditions see (Dorresteijn et al., 1993; Vervoort and Gazave, 2022)). Standard worms used in experiments were 3-4-month-old with 30-40 segments and were amputated according to the procedure detailed in (Planques et al., 2019; Vervoort and Gazave, 2022). In some experiments, regenerative parts were also re-amputated (either blastemas were totally removed, either regenerative parts were amputated in their middle, see Results section). At given time points reported in the Results section, regenerative parts as well as two posterior-most segments were collected and fixed in 4% paraformaldehyde (PFA) diluted in PBS Tween20 0.1% (PBT) for 2h at RT, then washed in PBT and gradually transferred in 100% Methanol at which point they can be stored at -20°C. For

fluorescent beads experiments, the regenerative parts were similarly collected and fixed but were not put in methanol and rather stored up to 24h in PBT at 4°C.

Histologic samples fixation, sectioning and fluorescent labelling

To perform histological sections, the samples were fixed in a solution of 4% PFA diluted in PBS 1X (without Tween20) for 1h30 at RT and washed in PBS 1X. Then, they were cryoprotected in a solution of sucrose diluted in PBS (300g/L) and stored for 4-5 days at 4°C. After the samples had settled in the sucrose solution, they were transferred into OCT embedding medium (Tissue Freezing Medium, Leica). The remaining sucrose was removed and the samples were put into molds and positioned according to the desired type of section (transverse or longitudinal). The samples were subsequently frozen with dry ice and stored inside the molds at -80°C. The sectioning was performed with a microtome (Leica CM3050S). Sections of 12-14µm were collected on SuperFrost glass slides and stored at -80°C. For *in situ* hybridizations on slices experiments, samples were fixed in a solution of 3.7% Formaldehyde, 0.2% Glutaraldehyde diluted in 1X PBT, then similarly cryoprotected, embedded, frozen and cut into 10µm slices. The cross-sections were then processed for immunostaining (Briscoe et al., 2000) with mouse anti-acetylated tubulin (Demilly et al 2013, Sigma T7451, 1:500), phalloidin labelling (Cytoskeleton, PHDR1; 1/500), *in situ* hybridization or EdU labelling (see below).

EdU, BrdU and EdU+BrdU cell proliferation assays

Proliferating cells in S-phase were labelled by incubating the worms with the thymidine analogs EdU (5-Ethynyl-2'-deoxy-Uridine) and/or BrdU (Bromo-deoxy-Uridine), at a respective concentration of 50µM and 1mM in natural fresh sea water (NFSW). Various incubation conditions (duration and biological stage) and pulse and chase experiments were performed as described in the Results section and related figures. The samples were then fixed and sections produced as described above. Briefly for EdU and/or BrdU labelling, after rehydration, the samples were digested with Proteinase K (40µg/mL for 10min); then the enzyme was inactivated with 2mg/mL Glycine in PBT (1 min) and the samples

post-fixed with 4% PFA in PBT (20 min) and washed with PBT. EdU-labelled cells were fluorescently marked by click-it chemistry with the specific addition of a fluorescent azide on EdU molecules (Click-iT™ EdU Cell Proliferation Kit, 488 or 555 dye, ThermoFisher, #C10337 and #C10638), following (Demilly et al., 2013; Vervoort and Gazave, 2022) procedure. For EdU labelling on sections, samples were shortly permeabilized in PBS Triton 0.1% before the click-it reaction. BrdU-labelled cells were marked by immunohistochemistry (primary antibody: MoBU-1, mouse, 1:250, ThermoFisher #B35128; secondary antibody: anti-mouse IgG Alexa Fluor® 555 Conjugate, 1:500, goat, Cell Signaling #4409). First, they underwent an antigen retrieval treatment with hydrochloric acid (final concentration of 2M diluted in distilled water for 1h at RT) and were incubated with the antibodies after a blocking step in a solution of sheep serum diluted in PBT. Dual labellings with EdU and BrdU were performed according to a method previously described in (Liboska et al., 2012). The EdU sites were first marked as described above, and the remaining un-labelled EdU sites were then saturated by click-it chemistry with an excess of non-fluorescent azide (Azido-methyl-phenyl-sulfide 95%, Sigma, #244546): the reaction was prepared and achieved according to the manufacturer's recommendations except the standard fluorescent azide was replaced by the non-fluorescent one at a final concentration of 2mM. The samples were then incubated in hydrochloric acid and the BrdU sites were bound by immunohistochemistry as described previously.

EdU cumulative labelling

Total cell cycle length (Tc), S-Phase length (Ts) and growth fraction (GF or proportion of proliferative cells) were determined by a cumulative labelling experiment with EdU as defined in (Nowakowski et al., 1989; Locker and Perron, 2019) and using the Excel spreadsheet provided by Dr R. Nowakowski. Non-amputated worms (from n=9 to 13) were exposed to 5µM EdU during increasing exposure times, until all proliferative cells are labeled (1, 5, 10, 16, 24, 48 and 72 h). Proportion of EdU+ cells were determined at three different positions, segments 1, 6 and 7 for two types of tissues: the gut and other trunk tissues (see cell counting section).

Probe synthesis and colorimetric *in situ* hybridization

Probe synthesis and colorimetric whole mount *in situ* hybridization (WMISH) were performed as described in (Demilly et al., 2013; Vervoort and Gazave, 2022). As detailed above for EdU and/or BrdU labelling, after rehydration, the samples were first digested with Proteinase K and post-fixed with PFA. Following that, the samples were pre-hybridized in hybridization buffer at 65 °c (1.5 h), and then incubated with the DIG-labelled probes overnight at 65 °C. DIG was then bound to specific antibodies bearing alkaline phosphatase and the tissues stained thanks to the cleavage of NBT (Nitro Blue Tetrazolium chloride) by this enzyme, catalysed by BCIP (5-Bromo-4-chloro-3-indolyl phosphate). WMISH meant to be observed by bright-field microscopy were mounted in Glycerol. WMISH meant to be observed by confocal microscopy thanks to the reflection procedure (see below) were nuclei counter-stained with Hoechst 0.1% overnight at 4°C and mounted in Glycerol/DABCO (2.5mg/ml DABCO in glycerol). *In situ* hybridization on slices were done similarly, with the following specificities: samples were digested using PBT + 0.2 % Triton for 20 mins. During hybridization step, samples were covered using parafilm to avoid evaporation of the probes. When combined with EdU labelling, the ISH was first performed just as described (whole mount or slice). After the coloration with NBT/BCIP, the EdU-labelled cells were fluorescently marked by click-it chemistry as described previously, and then all the nuclei were counter-stained with Hoechst and finally mounted in glycerol/DABCO.

In vivo gut cell labelling with fluorescent beads

To perform *in vivo* labelling of worm gut cells, we used 1µM-diameter fluorescent beads (Fluoresbrite® PolyFluor® 570 Microspheres, Polysciences, #24061-10) that were ingested by the worms. Worms were incubated in a solution of beads diluted in NFSW (1:100) for a week in 24-well plate, one worm per well, in the absence of food. After incubation, worms were rinsed with NFSW to remove non-ingested beads and individually monitored with a fluorescent binocular microscope to determine at which point the gut was marked with fluorescent beads, as the gut is never entirely labelled (the

terminal part is always beads-free). Posterior amputations were then performed just anterior to the bead labelling limit, and the worms were let to regenerate in NFSW complemented with food for specific times, depending on the following experiments (see Results section and associated figures). Samples were then collected, counter-stained with Hoechst and mounted in Glycerol/DABCO. When combined with *in vivo* gut cell labelling, EdU labelling was performed by click-it chemistry as seen previously, but for a shorter period of time (5min instead of 1h).

Procedure for tissue posteriorization

We established a procedure to label posterior gut cells (that do not incorporate fluorescent beads or for which EdU labelling is not specific) by giving a posterior identity to anterior tissues. We take advantage of the fact that after an amputation in an anterior segment, gut progenitors, labelled either with a 5h-long EdU pulse or with fluorescent beads, participate in the regeneration of gut cells which retain EdU and bead labellings when regeneration has finished. Unamputated worms are incubated either with fluorescent beads for a week, or with EdU for 5h, and amputated anteriorly shortly after. After 5 days of regeneration, a second amputation in the middle of the regenerated structure, removing the pygidium and growth zone that had regenerated after the first amputation, is done. Worms then regenerate a second time for 5 more days, before collection of the samples for further experiments. This regeneration procedure establishes a proxy of posteriorized gut epithelial cells, which are thus labelled. A schematic representation of the posteriorization procedure is available in Figure 3A.

Cell migration and proliferation inhibitors treatments

Cell proliferation was blocked using Hydroxy-Urea (HU) at 20 mM as previously described (Planques et al., 2019). Cell migration was blocked using LatrunculinB (LatB) at 20nM (as used in (Tweeten and Anderson, 2008)). HU and LatB were dissolved in sea water and DMSO, respectively. Both solutions were changed every 24h to maintain their activities for the duration of the experiment (5 days). Briefly,

individual worms were incubated in 2 ml of each solution (or control) on 12-wells plate. LatB-treated worms were scored every day for the regeneration stages that had been reached, as previously described (Planques et al., 2019; Vervoort and Gazave, 2022).

Imaging, acquisition and treatments

Bright-field images of colorimetric WMISH samples were acquired with a Leica CTR 5000 microscope. Fluorescent confocal images of WMISH samples were acquired with a Zeiss LSM780 microscope using a 633nm laser in reflection mode as described in (Jékely and Arendt, 2007). Other fluorescent confocal images were acquired with either a Zeiss LSM780 or LSM980 confocal microscope. Image processing (contrast and brightness, z-projection, auto-blend layers, transversal views) was performed with FIJI and Abode Photoshop. Figures were assembled with Adobe Illustrator.

EdU+ and/or BrdU+ cell counting

An automatic cell counting procedure was established and performed with the Imaris software by BitPlane (version 9.5). First, for each sample, all nuclei positions were identified and modelled thanks to the Hoechst signal by using the function “Spots” with a standardized nucleus diameter of 5µm. A Region of Interest (ROI) corresponding specifically, either to the regenerative part, a body segment or the gut was then manually delineated with the surface tool, also thanks to the Hoechst signal and the general morphology of the structure. Then, the spots inside the ROI were sorted along the fluorescent signals of the EdU or/and BrdU with a filter “Intensity Mean” to discriminate true positive nuclei from background. This procedure allowed to determine the absolute number of nuclei inside the ROI and, among them, the number of positive nuclei for each signal; and hence to extract the proportions of EdU+, BrdU+ and EdU+/BrdU+ cells for each sample.

Statistical analyses

All statistical tests and subsequent graphic representations were performed with GraphPad Prism 7. Mann–Whitney U tests were used to compare whole-blastema proportions of EdU+, BrdU+ and EdU+/BrdU+ cells between different experiments. Wilcoxon signed-rank tests were used to compare those proportions between different parts of the same sample. Multiple Mann–Whitney U tests were used to compare labelling index between the gut and other trunk tissues for all durations of EdU Pulse. Similarly, multiple Mann–Whitney U tests were used to compare LatB-treated and control worms for each day of treatment.

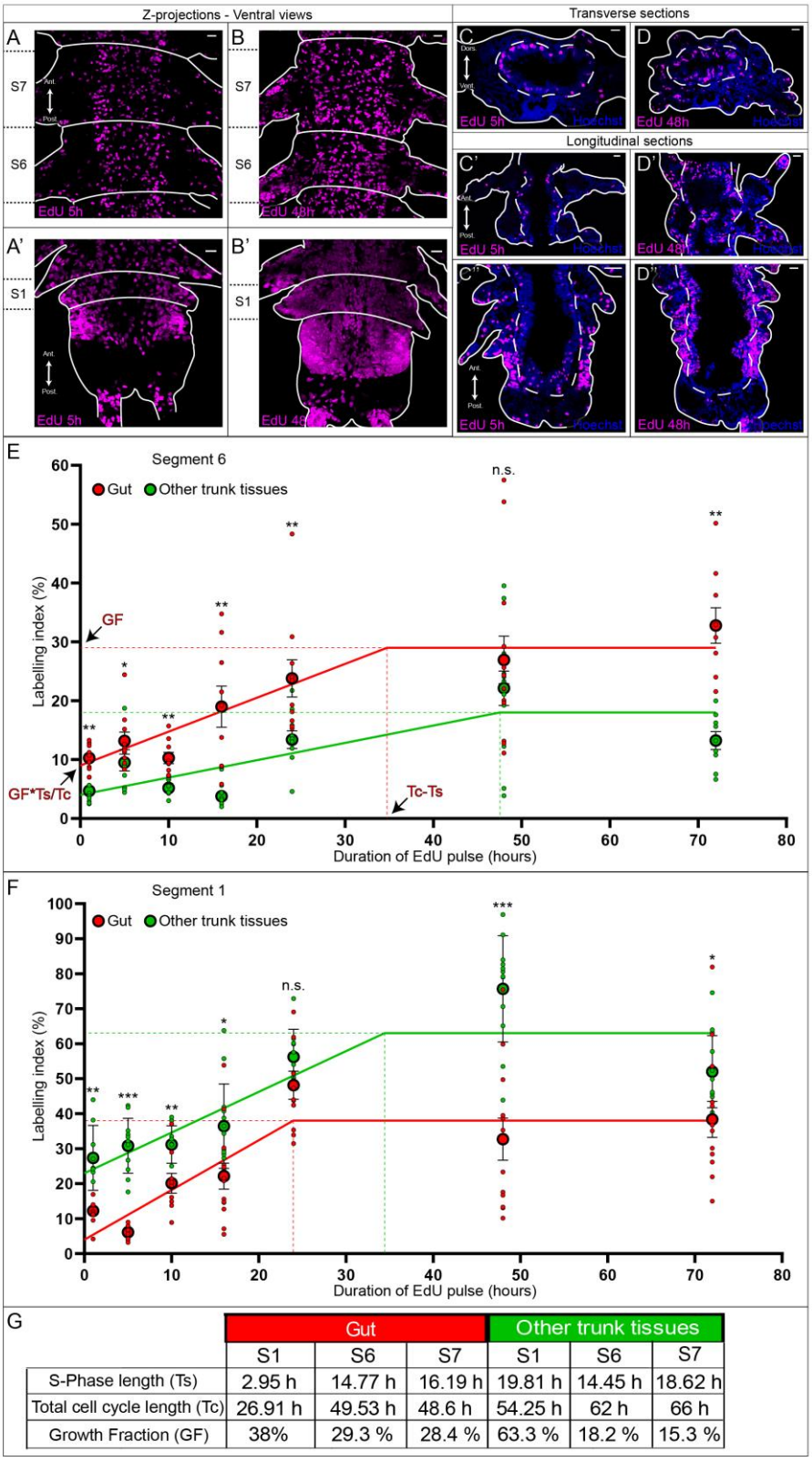

G

	Gut			Other trunk tissues		
	S1	S6	S7	S1	S6	S7
S-Phase length (Ts)	2.95 h	14.77 h	16.19 h	19.81 h	14.45 h	18.62 h
Total cell cycle length (Tc)	26.91 h	49.53 h	48.6 h	54.25 h	62 h	66 h
Growth Fraction (GF)	38%	29.3 %	28.4 %	63.3 %	18.2 %	15.3 %

Figure 1: Tracing the proliferative cells and assessing their cell cycle kinetics within different trunk tissues in *Platynereis* during continuous growth

(A-D) Distribution of EdU+ cells (magenta) and Hoechst DNA staining (blue) in the indicated segments of unamputated worms after 5h or 48h of EdU incorporation (5µM). (A- B') Confocal z-stacks (ventral views), (C, D) transversal cross-sections and (C'-D'') longitudinal ones. Anterior is up. White dashed lines: gut lining. Solid white lines: sample outline. Scale bar = 20µm. **(E, F)** EdU cumulative labelling index within the gut (red) and other trunk tissues (green), along the EdU exposure times, for S6 (E) and S1 **(F)**. Graphs generated using Nowakowski et al., 1989 spreadsheet. Small dots: individual values, large dots: means +- SD. N=9-13 segments analyzed *per* time point, *per* tissue. **(G)** Estimates of S-phase length (Ts), total cell cycle length (Tc) and growth fraction (GF). Mann-Whitney tests, * $p < 0.05$, ** $p < 0.01$, *** $p < 0.001$.

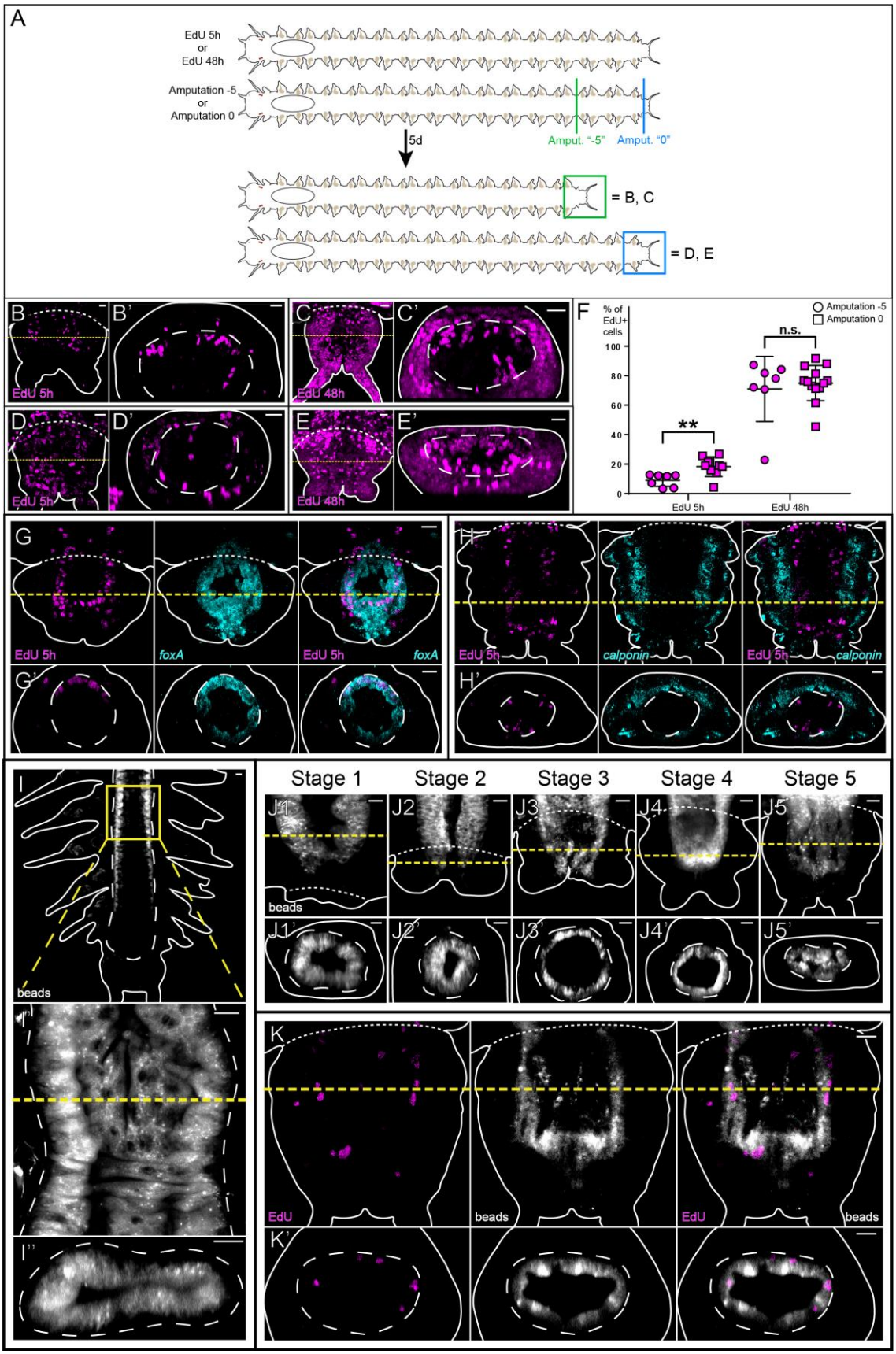

Figure 2: Gut progenitors localized anteriorly in the worm body are participating in regeneration and are lineage-restricted

A) Schematic representation of the experiment displayed in B to E. Incubation of unamputated worms with EdU for 5h or 48h, then amputation at two different positions: "-5" (removing five segments and the pygidium, in green) or "0" (removal of only the pygidium and the growth zone, in blue). The worms were then left to regenerate for 5 days. **(B-E)** Confocal z-stacks of regenerative parts at stage 5 after either a 5h-long EdU pulse and an amputation "-5" (B) or "0" (D); or after a 48h EdU pulse and an amputation "-5" (C) or "0" (E) (dorsal views, anterior is up). Corresponding virtual transverse sections (along the yellow dotted lines) shown in B', C', D' and E' respectively (dorsal is up). **(F)** Proportions of EdU+ cells after specified EdU pulses and amputation types (circle = amputation "-5", square = amputation "0"). Bracket: Mann-Whitney U test. n.s.; p >0.05; ** p<0.01. Mean +- SD are shown. **(G-H)** Confocal z-stacks of regenerative parts at stage 5 showing EdU+ cells (after a 5h-long EdU pulse prior to an amputation "-5", magenta) and *in situ* hybridization signal (cyan) for a gut (*foxA,* (G)) and a smooth muscle marker (*calponin,* (H)). Single and combined labelling displayed (dorsal views; anterior is up). Corresponding virtual transverse sections (along the yellow dotted lines) shown in G' and H' respectively (dorsal is up). **(I-K)** Unamputated juvenile worms incubated with fluorescent beads for a week and collected just before an anterior amputation (I-I'') or after 1 to 5 days of regeneration (J-K). **(I)** Confocal z-stack a worm's posterior part labelled with fluorescent beads (white) before amputation (dorsal view; anterior is up). A slight artefactual staining is visible in some parapodial glands. **(I')** Gut-focused magnification along the yellow box in I. **(I'')** Virtual transverse section along the yellow dotted line shown in I' (dorsal is up). **(J1-J5)** Confocal z-stacks of worms labelled with fluorescent beads (white) at the indicated stages of regeneration. Dorsal views are shown at the top (anterior is up). **(J1'-J5')** Virtual transverse section along the yellow dotted lines shown at the bottom (dorsal is up). **(K)** Confocal z-stacks of a stage 5 regenerative part after a dual beads/EdU labelling (dorsal view, anterior is up). **(K')** Virtual transverse section along the yellow dotted line shown in K(dorsal is up). White dashed lines: gut lining, solid white lines: sample outlines, yellow dotted lines: virtual sections planes, white dotted lines: amputation planes. Scale bar = 20µm.

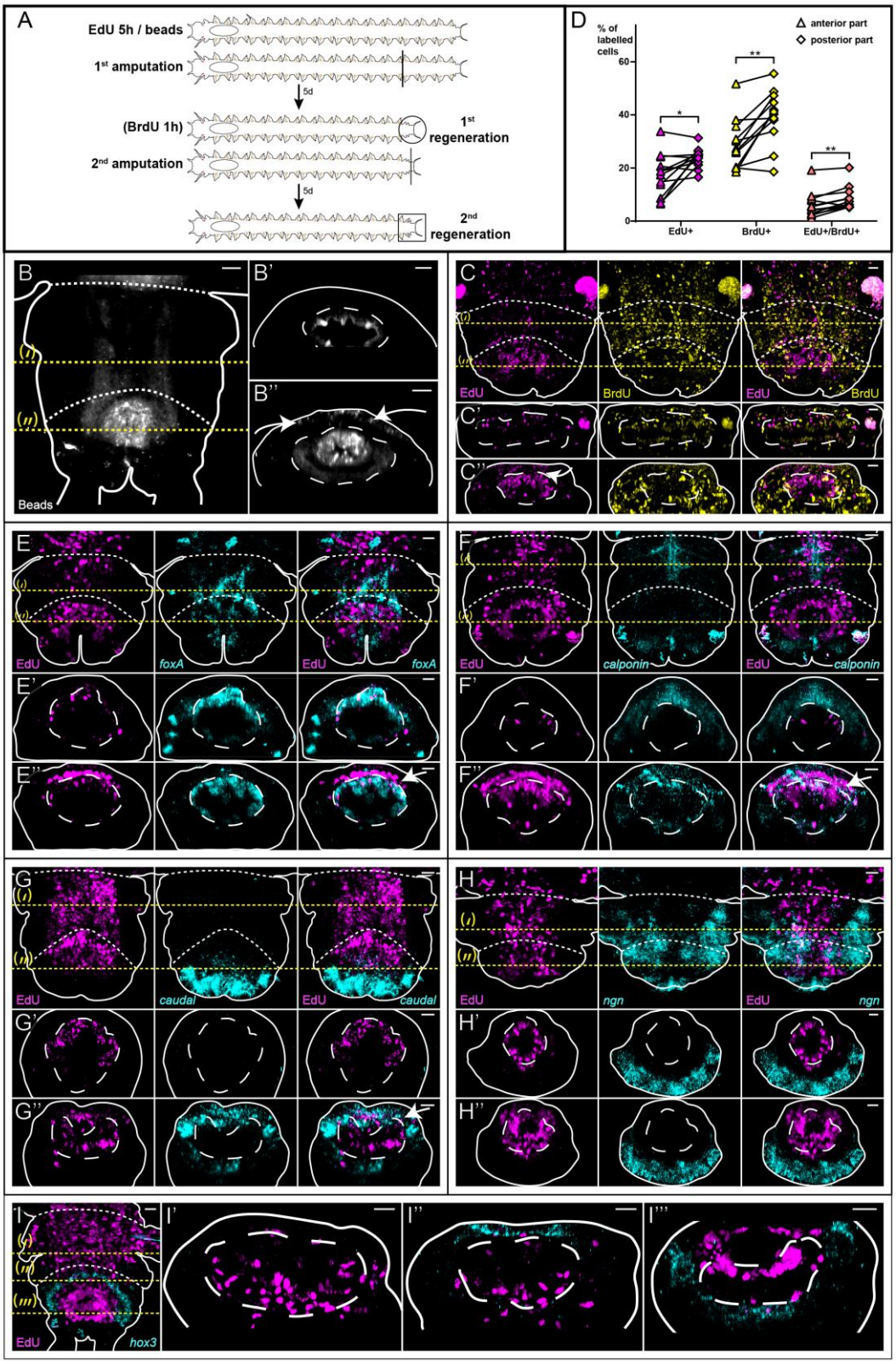

Figure 3: Posterior gut progenitors are more plastic

(A) Schematic of experimental procedure: unamputated juvenile worms incubated with fluorescent beads (1 week) or with EdU (5h) just before an anterior amputation. The worms were left to regenerate

for 5 days and some were also incubated with BrdU (1h). The regenerative parts (1st regeneration event, see Fig. 2) were re-amputated in the middle (*i.e.* removal of the regenerated pygidium and growth zone) and let to regenerate for 5 more days (2nd regeneration). **(B)** Confocal z-stack of a regenerative part obtained after both amputations described in A were performed on worms labelled with fluorescent beads (white) (dorsal view; anterior is up). **(B', B'')** Virtual transverse sections along the yellow dotted lines (') and ('') in B (dorsal is up). **(C)** Confocal z-stacks of a regenerative part obtained after both the amputations described in A were performed on worms incubated with EdU (magenta) and BrdU (yellow) (dorsal view; anterior is up). **(C', C'')** Virtual transverse sections along the yellow dotted lines (') and ('') shown in C (dorsal is up). **(D)** Comparison of EdU+, BrdU+ and EdU+/BrdU+ cell proportions between the anterior (triangle) and posterior (diamond) parts of samples from C (Wilcoxon signed-rank test: * $p < 0.05$; ** $p < 0.01$). **(E-I)** Confocal z-stacks of regenerative parts obtained after both amputations described in A were performed on worms incubated with EdU (dorsal views, anterior is up). *In situ* hybridization signals (cyan) for gut (*foxA,* (E)), smooth muscle (*calponin,* (F)), pygidium (*caudal,* (G)), neural (*neurogenin or ngn,* (H)), or growth zone (*hox3*, (I)) markers. **(E'- H', E''- H'')** Virtual transverse sections along the yellow dotted lines (') and ('') shown in E – H (dorsal is up). **(I'-I''')** Virtual transverse sections along the yellow dotted lines ('), (''), (''') shown in I (dorsal is up). White dashed lines: gut lining, solid white lines: sample outlines, yellow dotted lines: the virtual sections planes, white dotted lines: amputation planes, white arrows: fluorescent beads and EdU+ cells located outside the gut. Scale bar = 20µm.

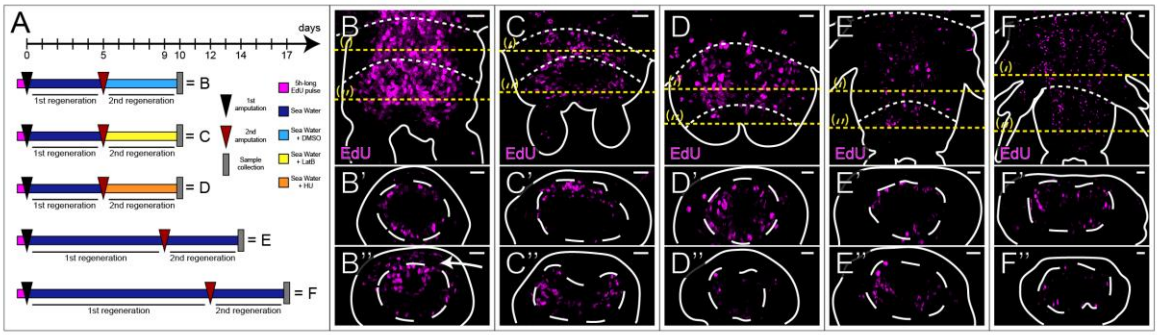

Figure 4: Cell proliferation and migration, as well as tissue maturity modulate the plasticity of posteriorized gut progenitors through regeneration

(A) Schematic of experimental procedure: worms were incubated in EdU (5h) prior to a 1st amputation "-5" (removing five segments and the pygidium). After 5, 9 or 12 dpa, a 2nd amputation was performed in the middle of the regenerated structure. The second regeneration event was performed in sea water either supplemented with DMSO (B, control) or with pharmacological inhibitors (C, LatrunculinB or LatB; D, Hydroxy-Urea or HU). **(B-F)** Confocal z-stacks of regenerative parts obtained after the procedure described in A are shown on the top (dorsal views, anterior is up). **(B'-F', B''-F'')** Virtual transverse sections along the yellow dotted lines (') and ('') shown in B-E (dorsal is up). White dashed lines: gut lining, solid white lines: sample outlines, yellow dotted lines: virtual sections planes, white dotted lines: amputation planes. Scale bar = 20 µm.

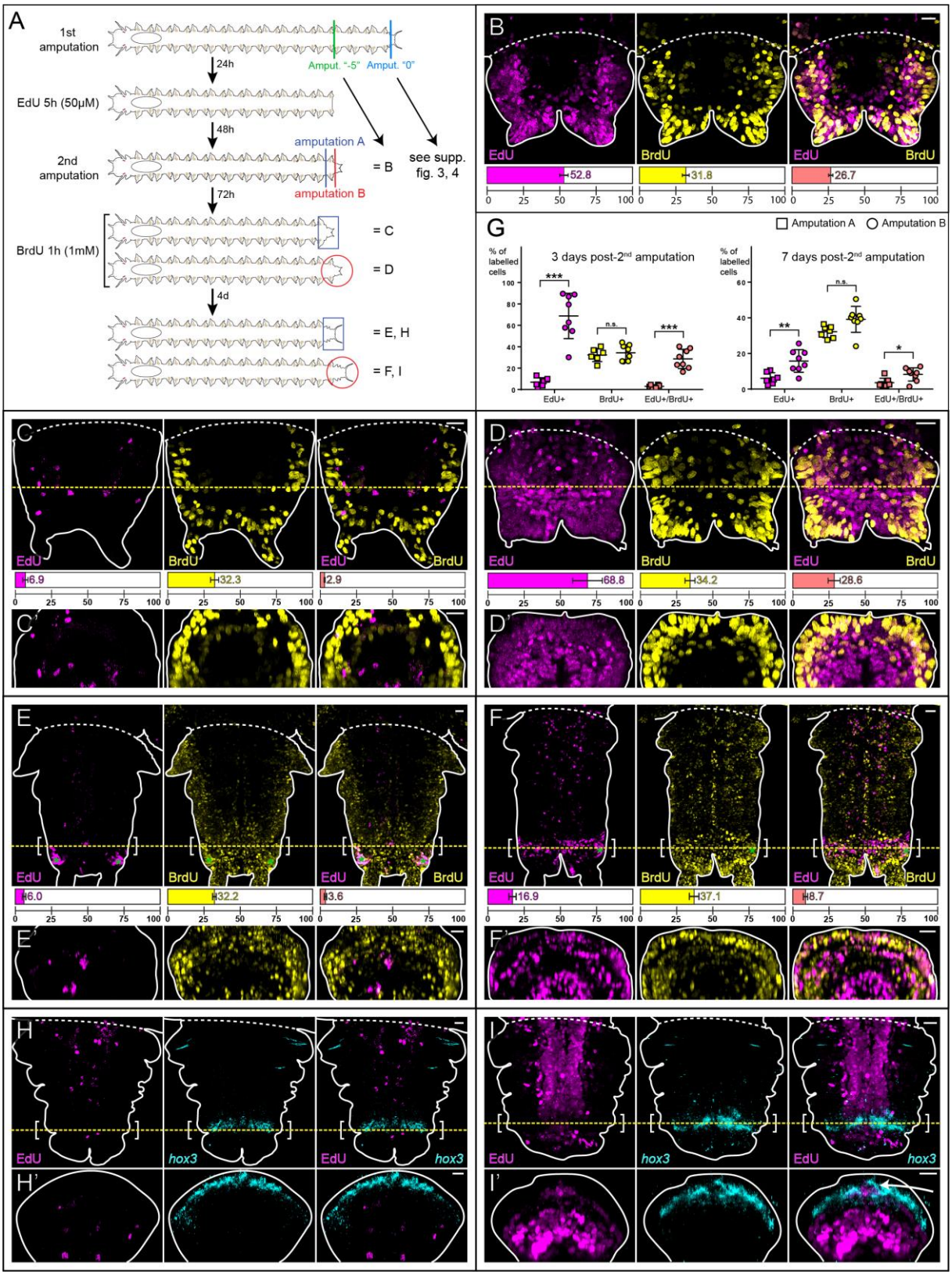

Figure 5: Most blastema cells originate from the segment abutting the amputation including the stem cells of the regenerated growth zone

(A) Schematic of experimental procedure: worms were amputated anteriorly (amputation "-5": removing five segments and the pygidium), left to regenerate for 24h, then incubated with EdU (5h) and left to regenerate for an additional 48h. Some were incorporated with BrdU (1h) (B). The other worms were then re-amputated removing either: the blastema and abutting segment (=amputation A) (C, E and H), or only the blastema(=amputation B) (D, F and I). The worms were then left to regenerate for three days, incubated with BrdU (1h) and collected (C and D) or left to regenerate for four more days (E and F). Others were just left to regenerate for seven days after the 2nd amputation (H and I). **(B)** Confocal z-stacks of a regenerative part obtained after an amputation "-5", incubated with EdU (magenta) at 1dpa and BrdU (yellow) at 3dpa (ventral view, anterior is up). **(C-F)** Confocal z-stacks of regenerative parts obtained after both amputations described in A were performed on worms incubated with EdU (magenta) and BrdU (yellow), (ventral views; anterior is up). **(C'-F')** Virtual transverse sections along the yellow dotted lines shown in C-F (ventral is up). **(G)** Comparisons of EdU+, BrdU+ and EdU+/BrdU+ cell proportions between samples at 3 days post-2nd amputation (C and D) on the left and at 7 days post-2nd amputation (E and F) on the right (square = amputation A; circle = amputation B). Bracket: Mann-Whitney U test. n.s. $p > 0.05$; * $p < 0.05$; ** $p < 0.01$; *** $p < 0.001$. Mean +- SD are shown. **(H-I)** Confocal z-stacks of regenerative parts at 7 days post-2nd amputation showing EdU+ cells (magenta) and *in situ* hybridization signal (cyan) for *hox3* (ventral views, anterior is up). Corresponding virtual transverse sections (along the yellow dotted lines) shown in H' and I' (ventral is up). Solid white lines: sample outlines, yellow dotted lines: virtual sections planes, white dotted lines: amputation planes. White brackets: growth zone, green asterisks: artefactual staining of pygidial glands. Scale bar = 20µm.

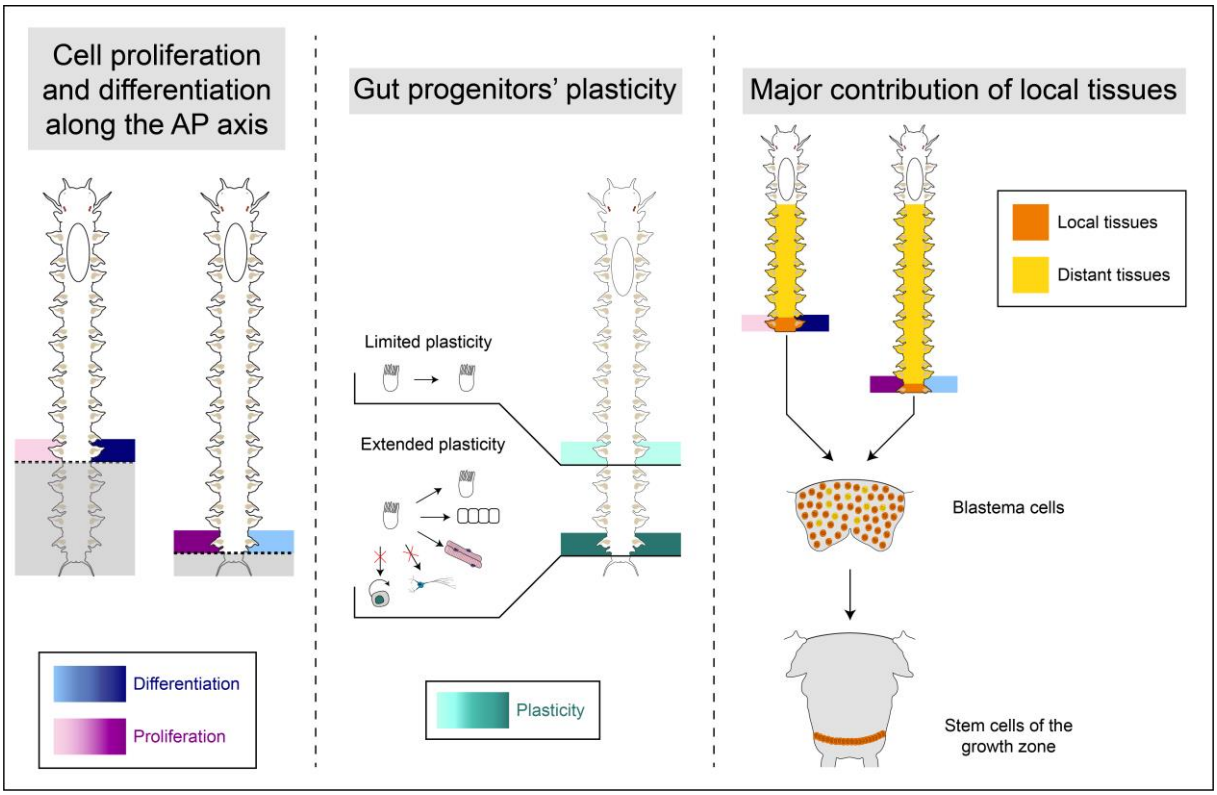

Figure 6: Cellular model for posterior regeneration in *Platynereis dumerilii*

Different levels of cell proliferation and differentiation shape tissue maturity and gut plasticity along the antero-posterior (AP) axis of the worms. Anterior amputation results in lineage-restricted gut progenitors producing only gut epithelial cells. Upon posteriorization, gut progenitors contribute to ectodermal and mesodermal tissues in addition to gut epithelial cells, thus exhibiting increased cell plasticity. Gut progenitors' plasticity is however limited as no posterior stem cells nor neural derivatives appear to be produced upon metaplasia. Regardless of amputation position along the AP axis, tissues abutting the amputation plane massively contribute to blastema formation and regeneration of growth zone stem cells. The left panel illustrates varying levels of cell proliferation (magenta) and tissue differentiation (blue). Different degrees of gut progenitors' plasticity are depicted in the middle panel. Local (orange) and distant (yellow) tissues are depicted in the right panel.

Acknowledgments

This study is dedicated to the memory of our friend, mentor and supervisor, the late Professor Michel Vervoort. We are grateful to all members of the Gazave & Vervoort lab for their support and suggestions on this study. We deeply thank Dr. Quentin Schenkelaars for suggesting the use of fluorescent beads, as well as Dr. Gabriel Krasovec and Dr. Lucie Laplane for helpful comments on the manuscript. We thank Dr. Yves Clément for his help with statistical analyses. We are grateful to Dr Roger Karess for his diligent proofreading of the manuscript. We acknowledge the ImagoSeine core facility of Institut Jacques Monod, member of France-BioImaging (ANR-10-INBS-04) and IBiSA, with the support of Labex "Who Am I", Inserm Plan Cancer, Region Ile-de-France and Fondation Bettencourt Schueller. We are grateful to the staff of the animal facility for their help with the *Platynereis'* culture.

Conflict of Interests

The authors declare that they have no conflict of interest.

Funding

Work in our team is supported by funding from: Labex “Who Am I” laboratory of excellence (No. ANR-11-LABX-0071) funded by the French Government through its “Investments for the Future” program operated by the Agence Nationale de la Recherche under grant No. ANR-11-IDEX-0005-01, Agence Nationale de la Recherche «STEM» (ANR-19-CE27-0027-01)), Centre National de la Recherche Scientifique (CNRS), INSB (Grant Diversity of Biological Mechanisms), Université Paris Cité, Association pour la Recherche sur le Cancer (grant PJA 20191209482), and comité départemental de Paris de la Ligue Nationale Contre le Cancer (grant RS20/75-20). LB has obtained a CDSN PhD fellowship from ENS Lyon and his fourth year of PhD is supported by the Labex “Who am I”.

Bibliography

Álvarez-Campos, P., García-Castro, H., Emili, E., Pérez-Posada, A., Salamanca-Díaz, D.A., Mason, V., Metzger, B., Bely, A.E., Kenny, N., Özpolat, B.D., Solana, J., 2023. Annelid adult cell type diversity and their pluripotent cellular origins. bioRxiv 2023.04.25.537979. https://doi.org/10.1101/2023.04.25.537979

Azevedo, A.S., Grotek, B., Jacinto, A., Weidinger, G., Saúde, L., 2011. The regenerative capacity of the zebrafish caudal fin is not affected by repeated amputations. PLoS One 6, e22820. https://doi.org/10.1371/journal.pone.0022820

Bely, A.E., 2014. Early events in annelid regeneration: a cellular perspective. Integr Comp Biol 54, 688–699. https://doi.org/10.1093/icb/icu109

Bely, A.E., 2006. Distribution of segment regeneration ability in the Annelida. Integrative and Comparative Biology 46, 508–518. https://doi.org/10.1093/icb/icj051

Bely, A.E., Nyberg, K.G., 2010. Evolution of animal regeneration: re-emergence of a field. Trends Ecol. Evol. (Amst.) 25, 161–170. https://doi.org/10.1016/j.tree.2009.08.005

Bideau, L., Kerner, P., Hui, J., Vervoort, M., Gazave, E., 2021. Animal regeneration in the era of transcriptomics. Cell. Mol. Life Sci. 78, 3941–3956. https://doi.org/10.1007/s00018-021-03760-7

Blanpain, C., Fuchs, E., 2014. Plasticity of epithelial stem cells in tissue regeneration. Science 344, 1242281. https://doi.org/10.1126/science.1242281

Boilly, B., Boilly-Marer, Y., Bely, A.E., 2017. Regulation of dorso-ventral polarity by the nerve cord during annelid regeneration: A review of experimental evidence. Regeneration (Oxf) 4, 54–68. https://doi.org/10.1002/reg2.78

Briscoe, J., Pierani, A., Jessell, T.M., Ericson, J., 2000. A Homeodomain Protein Code Specifies Progenitor Cell Identity and Neuronal Fate in the Ventral Neural Tube. Cell 101, 435–445. https://doi.org/10.1016/S0092-8674(00)80853-3

Brunet, T., Fischer, A.H., Steinmetz, P.R., Lauri, A., Bertucci, P., Arendt, D., 2016. The evolutionary origin of bilaterian smooth and striated myocytes. eLife 5, e19607. https://doi.org/10.7554/eLife.19607

Bryant, D.M., Sousounis, K., Payzin-Dogru, D., Bryant, S., Sandoval, A.G.W., Martinez Fernandez, J., Mariano, R., Oshiro, R., Wong, A.Y., Leigh, N.D., Johnson, K., Whited, J.L., 2017. Identification of regenerative roadblocks via repeat deployment of limb regeneration in axolotls. NPJ Regen Med 2, 30. https://doi.org/10.1038/s41536-017-0034-z

Caplan, A.I., Ordahl, C.P., 1978. Irreversible Gene Repression Model for Control of Development. Science 201, 120–130. https://doi.org/10.1126/science.351805

Cohen, E., Peterson, N.G., Sawyer, J.K., Fox, D.T., 2021. Accelerated cell cycles enable organ regeneration under developmental time constraints in the Drosophila hindgut. Developmental Cell 56, 2059-2072.e3. https://doi.org/10.1016/j.devcel.2021.04.029

Crucianelli, C., Jaiswal, J., Maya, A.V., Nogay, L., Cosolo, A., Grass, I., Classen, A.-K., 2022. Distinct signaling signatures drive compensatory proliferation via S-phase acceleration. PLOS Genetics 18, e1010516. https://doi.org/10.1371/journal.pgen.1010516

Dahlitz, I., Dorresteijn, A., Holz, A., 2023. Remodeling of the Platynereis Musculature during Sexual Maturation. Biology 12, 254. https://doi.org/10.3390/biology12020254

de Jong, D.M., Seaver, E.C., 2017. Investigation into the cellular origins of posterior regeneration in the annelid Capitella teleta. Regeneration (Oxf) 5, 61–77. https://doi.org/10.1002/reg2.94

de Rosa, R., Prud'homme, B., Balavoine, G., 2005. caudal and even-skipped in the annelid Platynereis dumerilii and the ancestry of posterior growth. Evolution & Development 7, 574–587. https://doi.org/10.1111/j.1525-142X.2005.05061.x

Demilly, A., Steinmetz, P., Gazave, E., Marchand, L., Vervoort, M., 2013. Involvement of the Wnt/β-catenin pathway in neurectoderm architecture in Platynereis dumerilii. Nat Commun 4, 1915. https://doi.org/10.1038/ncomms2915

Dorresteijn, A.W.C., O'Grady, B., Fischer, A., Porchet-Henneré, E., Boilly-Marer, Y., 1993. Molecular specification of cell lines in the embryo of Platynereis (Annelida). Rouxs Arch Dev Biol 202, 260–269. https://doi.org/10.1007/BF00363215

Eguchi, G., Eguchi, Y., Nakamura, K., Yadav, M.C., Millán, J.L., Tsonis, P.A., 2011. Regenerative capacity in newts is not altered by repeated regeneration and ageing. Nat Commun 2, 384. https://doi.org/10.1038/ncomms1389

Eming, S.A., Martin, P., Tomic-Canic, M., 2014. Wound repair and regeneration: Mechanisms, signaling, and translation. Sci Transl Med 6, 265sr6. https://doi.org/10.1126/scitranslmed.3009337

Flowers, G.P., Sanor, L.D., Crews, C.M., 2017. Lineage tracing of genome-edited alleles reveals high fidelity axolotl limb regeneration. eLife 6, e25726. https://doi.org/10.7554/eLife.25726

Friedl, P., Gilmour, D., 2009. Collective cell migration in morphogenesis, regeneration and cancer. Nat Rev Mol Cell Biol 10, 445–457. https://doi.org/10.1038/nrm2720

Galliot, B., Ghila, L., 2010. Cell plasticity in homeostasis and regeneration. Mol Reprod Dev 77, 837–855. https://doi.org/10.1002/mrd.21206

Gazave, E., Béhague, J., Laplane, L., Guillou, A., Préau, L., Demilly, A., Balavoine, G., Vervoort, M., 2013. Posterior elongation in the annelid Platynereis dumerilii involves stem cells molecularly related to primordial germ cells. Dev. Biol. 382, 246–267. https://doi.org/10.1016/j.ydbio.2013.07.013

Gazave, E., Lemaître, Q.I.B., Balavoine, G., 2017. The Notch pathway in the annelid Platynereis: insights into chaetogenesis and neurogenesis processes. Open Biol 7, 160242. https://doi.org/10.1098/rsob.160242

Gazave, E., Schenkelaars, Q., 2021. The Annelid Platynereis dumerilii as an Experimental Model for Evo-Devo and Regeneration Studies, in: Handbook of Marine Model Organisms in Experimental Biology. CRC Press.

Ghosh, M., Hill, C.L., Alsudayri, A., Lallier, S.W., Hayes Jr., D., Wijeratne, S., Tan, Z.H., Chiang, T., Mahoney, J.E., Carraro, G., Stripp, B.R., Reynolds, S.D., 2021. Repeated injury promotes tracheobronchial tissue stem cell attrition. STEM CELLS Translational Medicine 10, 1696–1713. https://doi.org/10.1002/sctm.21-0032

Govindasamy, N., Murthy, S., Ghanekar, Y., 2014. Slow-cycling stem cells in hydra contribute to head regeneration. Biol Open 3, 1236–1244. https://doi.org/10.1242/bio.201410512

Haller, S., Kapuria, S., Riley, R.R., O'Leary, M.N., Schreiber, K.H., Andersen, J.K., Melov, S., Que, J., Rando, T.A., Rock, J., Kennedy, B.K., Rodgers, J.T., Jasper, H., 2017. mTORC1 activation during repeated regeneration impairs somatic stem cell maintenance. Cell Stem Cell 21, 806-818.e5. https://doi.org/10.1016/j.stem.2017.11.008

Jékely, G., Arendt, D., 2007. Cellular resolution expression profiling using confocal detection of NBT/BCIP precipitate by reflection microscopy. Biotechniques 42, 751–755. https://doi.org/10.2144/000112462

Juliano, C.E., Swartz, S.Z., Wessel, G.M., 2010. A conserved germline multipotency program. Development 137, 4113–4126. https://doi.org/10.1242/dev.047969

Karmakar, S., Deng, L., He, X.C., Li, L., 2020. Intestinal epithelial regeneration: active versus reserve stem cells and plasticity mechanisms. American Journal of Physiology-Gastrointestinal and Liver Physiology 318, G796–G802. https://doi.org/10.1152/ajpgi.00126.2019

Koren, E., Feldman, A., Yusupova, M., Kadosh, A., Sedov, E., Ankawa, R., Yosefzon, Y., Nasser, W., Gerstberger, S., Kimel, L.B., Priselac, N., Brown, S., Sharma, S., Gorenc, T., Shalom-Feuerstein, R., Steller, H., Shemesh, T., Fuchs, Y., 2022. Thy1 marks a distinct population of slow-cycling stem cells in the mouse epidermis. Nat Commun 13, 4628. https://doi.org/10.1038/s41467-022-31629-1

Kragl, M., Knapp, D., Nacu, E., Khattak, S., Maden, M., Epperlein, H.H., Tanaka, E.M., 2009. Cells keep a memory of their tissue origin during axolotl limb regeneration. Nature 460, 60–65. https://doi.org/10.1038/nature08152

Lerchenberger, M., Uhl, B., Stark, K., Zuchtriegel, G., Eckart, A., Miller, M., Puhr-Westerheide, D., Praetner, M., Rehberg, M., Khandoga, A.G., Lauber, K., Massberg, S., Krombach, F., Reichel, C.A., 2013. Matrix metalloproteinases modulate ameboid-like migration of neutrophils through inflamed interstitial tissue. Blood 122, 770–780. https://doi.org/10.1182/blood-2012-12-472944

Liboska, R., Ligasová, A., Strunin, D., Rosenberg, I., Koberna, K., 2012. Most Anti-BrdU Antibodies React with 2'-Deoxy-5-Ethynyluridine — The Method for the Effective Suppression of This Cross-Reactivity. PLoS One 7, e51679. https://doi.org/10.1371/journal.pone.0051679

Lin, T.-Y., Gerber, T., Taniguchi-Sugiura, Y., Murawala, P., Hermann, S., Grosser, L., Shibata, E., Treutlein, B., Tanaka, E.M., 2021. Fibroblast dedifferentiation as a determinant of successful regeneration. Developmental Cell 56, 1541-1551.e6. https://doi.org/10.1016/j.devcel.2021.04.016

Locker, M., Perron, M., 2019. In Vivo Assessment of Neural Precursor Cell Cycle Kinetics in the Amphibian Retina. Cold Spring Harb Protoc 2019. https://doi.org/10.1101/pdb.prot105536

Merrell, A.J., Stanger, B.Z., 2016. Adult cell plasticity in vivo: de-differentiation and transdifferentiation are back in style. Nat Rev Mol Cell Biol 17, 413–425. https://doi.org/10.1038/nrm.2016.24

Mills, J.C., Stanger, B.Z., Sander, M., 2019. Nomenclature for cellular plasticity: are the terms as plastic as the cells themselves? EMBO J 38, e103148. https://doi.org/10.15252/embj.2019103148

Molinaro, A.M., Lindsay-Mosher, N., Pearson, B.J., 2021. Identification of TOR-responsive slow-cycling neoblasts in planarians. EMBO reports 22, e50292. https://doi.org/10.15252/embr.202050292

Myohara, M., Yoshida-Noro, C., Kobari, F., Tochinai, S., 1999. Fragmenting oligochaete Enchytraeus japonensis: a new material for regeneration study. Dev Growth Differ 41, 549–555. https://doi.org/10.1046/j.1440-169x.1999.00455.x

Nowakowski, R.S., Lewin, S.B., Miller, M.W., 1989. Bromodeoxyuridine immunohistochemical determination of the lengths of the cell cycle and the DNA-synthetic phase for an anatomically defined population. J Neurocytol 18, 311–318. https://doi.org/10.1007/BF01190834

Özpolat, B.D., Bely, A.E., 2016. Developmental and molecular biology of annelid regeneration: a comparative review of recent studies. Current Opinion in Genetics & Development, Cell reprogramming, regeneration and repair 40, 144–153. https://doi.org/10.1016/j.gde.2016.07.010

Özpolat, B.D., Randel, N., Williams, E.A., Bezares-Calderón, L.A., Andreatta, G., Balavoine, G., Bertucci, P.Y., Ferrier, D.E.K., Gambi, M.C., Gazave, E., Handberg-Thorsager, M., Hardege, J., Hird, C., Hsieh, Y.-W., Hui, J., Mutemi, K.N., Schneider, S.Q., Simakov, O., Vergara, H.M., Vervoort, M., Jékely, G., Tessmar-Raible, K., Raible, F., Arendt, D., 2021. The Nereid on the rise: Platynereis as a model system. Evodevo 12, 10. https://doi.org/10.1186/s13227-021-00180-3

Parain, K., Chesneau, A., Locker, M., Borday, C., Perron, M., 2023. Regeneration from three cellular sources and ectopic mini-retina formation upon neurotoxic retinal degeneration in Xenopus. bioRxiv 2023.05.12.540545. https://doi.org/10.1101/2023.05.12.540545

Planques, A., Malem, J., Parapar, J., Vervoort, M., Gazave, E., 2019. Morphological, cellular and molecular characterization of posterior regeneration in the marine annelid Platynereis dumerilii. Dev. Biol. 445, 189–210. https://doi.org/10.1016/j.ydbio.2018.11.004

Ramon-Mateu, J., Ellison, S.T., Angelini, T.E., Martindale, M.Q., 2019. Regeneration in the ctenophore Mnemiopsis leidyi occurs in the absence of a blastema, requires cell division, and is temporally separable from wound healing. BMC Biology 17, 80. https://doi.org/10.1186/s12915-019-0695-8

Randolph, H., 1892. The regeneration of the tail in lumbriculus. Journal of Morphology 7, 317–344. https://doi.org/10.1002/jmor.1050070304
Ribeiro, R.P., Egger, B., Ponz-Segrelles, G., Aguado, M.T., 2021. Cellular proliferation dynamics during regeneration in Syllis malaquini (Syllidae, Annelida). Frontiers in Zoology 18, 27. https://doi.org/10.1186/s12983-021-00396-y
Sandoval-Guzmán, T., Wang, H., Khattak, S., Schuez, M., Roensch, K., Nacu, E., Tazaki, A., Joven, A., Tanaka, E.M., Simon, A., 2014. Fundamental differences in dedifferentiation and stem cell recruitment during skeletal muscle regeneration in two salamander species. Cell Stem Cell 14, 174–187. https://doi.org/10.1016/j.stem.2013.11.007
Shalaeva, A.Y., Kozin, V.V., 2023. Cell Proliferation Indices in Regenerating Alitta virens (Annelida, Errantia). Cells 12, 1354. https://doi.org/10.3390/cells12101354
Sinigaglia, C., Averof, M., 2019. The multifaceted role of nerves in animal regeneration. Curr. Opin. Genet. Dev. 57, 98–105. https://doi.org/10.1016/j.gde.2019.07.020
Song, S., Starunov, V., Bailly, X., Ruta, C., Kerner, P., Cornelissen, A.J.M., Balavoine, G., 2020. Globins in the marine annelid Platynereis dumerilii shed new light on hemoglobin evolution in bilaterians. BMC Evol Biol 20, 165. https://doi.org/10.1186/s12862-020-01714-4
Sousounis, K., Qi, F., Yadav, M.C., Millán, J.L., Toyama, F., Chiba, C., Eguchi, Y., Eguchi, G., Tsonis, P.A., 2015. A robust transcriptional program in newts undergoing multiple events of lens regeneration throughout their lifespan. Elife 4, e09594. https://doi.org/10.7554/eLife.09594
Spector, I., Shochet, N.R., Kashman, Y., Groweiss, A., 1983. Latrunculins: Novel Marine Toxins That Disrupt Microfilament Organization in Cultured Cells. Science 219, 493–495. https://doi.org/10.1126/science.6681676
Steinmetz, P.R.H., Kostyuchenko, R.P., Fischer, A., Arendt, D., 2011. The segmental pattern of otx, gbx, and Hox genes in the annelid Platynereis dumerilii. Evolution & Development 13, 72–79. https://doi.org/10.1111/j.1525-142X.2010.00457.x
Stocum, D.L., Cameron, J.A., 2011. Looking proximally and distally: 100 years of limb regeneration and beyond. Dev. Dyn. 240, 943–968. https://doi.org/10.1002/dvdy.22553
Sugio, M., Yoshida-Noro, C., Ozawa, K., Tochinai, S., 2012. Stem cells in asexual reproduction of Enchytraeus japonensis (Oligochaeta, Annelid): Proliferation and migration of neoblasts. Development, Growth & Differentiation 54, 439–450. https://doi.org/10.1111/j.1440-169X.2012.01328.x
Tanaka, E.M., Reddien, P.W., 2011. The Cellular Basis for Animal Regeneration. Developmental Cell 21, 172–185. https://doi.org/10.1016/j.devcel.2011.06.016
Tilic, E., Herkenrath, T., Kirfel, G., Bartolomaeus, T., 2023. The cellular 3D printer of a marine bristle worm—chaetogenesis in Platynereis dumerilii (Audouin & Milne Edwards, 1834) (Annelida). Cell Tissue Res 391, 305–322. https://doi.org/10.1007/s00441-022-03731-9
Tiozzo, S., Copley, R.R., 2015. Reconsidering regeneration in metazoans: an evo-devo approach. Front. Ecol. Evol. 3. https://doi.org/10.3389/fevo.2015.00067
Tornini, V.A., Thompson, J.D., Allen, R.L., Poss, K.D., 2017. Live fate-mapping of joint-associated fibroblasts visualizes expansion of cell contributions during zebrafish fin regeneration. Development 144, 2889–2895. https://doi.org/10.1242/dev.155655
Tweeten, K.A., Anderson, A., 2008. Analysis of cell proliferation and migration during regeneration in Lumbriculus variegatus (Clitellata: Lumbriculidae). bios 79, 183–190. https://doi.org/10.1893/0005-3155-79.4.183
Varley, Á., Horkan, H.R., McMahon, E.T., Krasovec, G., Frank, U., 2023. Pluripotent, germ cell competent adult stem cells underlie cnidarian regenerative ability and clonal growth. Curr Biol 33, 1883-1892.e3. https://doi.org/10.1016/j.cub.2023.03.039
Vervoort, M., Gazave, E., 2022. Studying Annelida Regeneration Using Platynereis dumerilii. Methods Mol Biol 2450, 207–226. https://doi.org/10.1007/978-1-0716-2172-1_11
Virchow, R., 1886. Congrès périodique international des sciences médicales. 8th session, Copenhague 1884. F. Hegel & fils.

Wagner, D.E., Wang, I.E., Reddien, P.W., 2011. Clonogenic neoblasts are pluripotent adult stem cells that underlie planarian regeneration. Science 332, 811–816. https://doi.org/10.1126/science.1203983

Wenemoser, D., Reddien, P.W., 2010. Planarian regeneration involves distinct stem cell responses to wounds and tissue absence. Developmental Biology 344, 979–991. https://doi.org/10.1016/j.ydbio.2010.06.017

Yan, S.L.S., Hwang, I.-Y., Kamenyeva, O., Kehrl, J.H., 2019. In Vivo F-Actin Filament Organization during Lymphocyte Transendothelial and Interstitial Migration Revealed by Intravital Microscopy. iScience 16, 283–297. https://doi.org/10.1016/j.isci.2019.05.040

Žídek, R., Machoň, O., Kozmik, Z., 2018. Wnt/β-catenin signalling is necessary for gut differentiation in a marine annelid, Platynereis dumerilii. EvoDevo 9, 14. https://doi.org/10.1186/s13227-018-0100-7